DOI: 10.53704/fujnas.v8i2.270

A publication of College of Natural and Applied Sciences, Fountain University, Osogbo, Nigeria.
Journal homepage: www.fountainjournals.com
ISSN: 2354-337X(Online),2350-1863(Print)

Spray Pyrolysis Deposition and Characterisation of Dielectric SnO_2 Thin Films

[*1,2]Animasahun, L. O., [2]Taleatu, B. A., [1]Bolarinwa, H. S., [3]Fasasi, A. Y., [2]Eleruja, M. A., [3]Obiajunwa E. I. and [3]Pelemo D.

[1] Department of Physics, Electronics, and Earth Sciences, Fountain University, Osogbo, Nigeria
[2] Department of Physics & Engineering Physics, Obafemi Awolowo University, Ile-Ife, Nigeria
[3] Centre for Energy Research & Development, Obafemi Awolowo University, Ile-Ife, Nigeria.

Abstract

Dielectric and optical dispersion properties of thin films of SnO_2 deposited via spray pyrolysis were investigated. These properties are fundamental to new applications of SnO_2 in energy storage and pressure sensing. The composition and thickness of the films were determined using the Rutherford Backscattered Spectroscopic mode of the Pelletron Tandem Accelerator. X-ray diffraction (XRD) technique and scanning electron microscope (SEM) were used to examine the crystal structure and surface morphology of the films. Optical transmission data were analyzed to obtain the optical band gap, dispersion parameters, and dielectric constants. The analyses showed that the films were polycrystalline in nature with the tetragonal rutile crystal structure. It was also observed that annealed films increased in thickness compared to the as-deposited samples. The Urbach tail width of the annealed sample also decresed from 293 to 252 meV indicating an improvement in crystallinity with heat treatment. The refractive index dispersion in the visible region analyzed in terms of long wavelength single-oscillator Sellmier approximation was in the range 1.9 -3.0. The zero and high-frequency dielectric constants were evaluated. The values of these constants could be a justification for further exploration of SnO_2-based materials for charge storage and capacitive pressure sensing.

Keywords: pyrolysis, dielectric, refractive index, thin films

Introduction

SnO_2 is a wide bandgap semiconducting dielectric material. It belongs to a class of materials that combines high electrical conductivity with optical transparency and thus constitutes an important component for optoelectronic applications such as flat panel displays, solar cells, photodetectors, LEDs and transistors (Abdullah *et al.*, 2012; Bancolo *et al*., 2012 and Batal *et al.,* 2012). It is the most commonly used metal oxide gas sensing material (Brousseau *et al.,* 1997; Batzill & Diebold, 2005; Borse & Garde, 2008; Caglar *et al*., 2007; Chani, *et al*., 2015). As a dielectric material it has been explored in fabricating capacitors/supercapacitors for energy storage, supplying burst of power to devices and components and for filtering (Edukondalu *et al*.,1992; Gordillo, *et al*., 1994; Galatsis, *et al*., 2003; Fasasi *et al*., 2009; Chen *et al.*, 2012; Guan

*Corresponding author: +2349063395212
Email address: luqman.animasahun@gmail.com

et al., 2014 and He *et al*., 2014). There are other applications of SnO_2-based dielectrics such as sensors like strain gauge and electrical insulation in wire and cable protection (Hu *et al*., 2009). In all these applications, it is obvious that the dispersion characteristics and dielectric constants are two important parameters to determine. For instance, the larger the dielectric constant the more energy the capacitor can store with other factors being favourable. In addition, the dielectric change will influence the features and efficiency of the devices, such as thermal loss, current leakage, refractive index, signal response speed, and light transmittance. Despite its wide areas of dielectric applications there are few studies on its dielectric and dispersion properties (Jarzebski & Morton, 1976; Korotcenkov *et al*., 2001; Lim *et al*., 2008; Li, *et al*., 2009; Liu *et al*., 2012 and Ikhmayies & Ahmad-Bitar, 2013).

Tin oxide films, nano-sized tin oxide particles and nanostructured tin oxides have been produced by a variety of synthesis techniques such as sol-gel processing Liu *et al* (2012), e-beam evaporation Wu, *et al* (2014), thermal co-evaporation, Melsheimer & Ziegler (1985), hydrothermal Natsume *et al* (1995), screen printing Park *et al* (2011), ion irradiation Shine *et al* (2011), gas phase condensation Perednis & Gauckler (2005), mechanochemical processing Pusawale *et al* (2011), and spray pyrolysis (Serin *et al*., 2006; Gedanken *et al*., 2008 and Wang *et al*., 2014). The choice of a synthesis method depends on a number of important factors. These include but not limited to the cost of materials and procedures required, repeatability of properties, scalability for industrial production, continuous versus batch processing, and the number, complexity, and waste associated with the fabrication steps (Chani *et al.*, 2015). In order to obtain uniform and quality films of the oxide, we used the chemical spray pyrolysis method. The spray pyrolysis process is a simple and low-cost technique for ceramic thin films deposition and nanometer-sized powder production (Zhang *et al*., 2018). The process equipment is rather simple; the method is robust and if properly controlled yields oxide films of high quality at rather low costs. This process has the potential to produce thin layers on different substrates (Zhang *et al*., 2018).

Therefore, in this study, SnO_2 films were deposited on glass substrates by spray pyrolysis method. The optical and dielectric parameters such as the static (zero frequency) and high-frequency dielectric constants and the refractive index dispersion were investigated. These are important parameters for device fabrication and simulation for various energy and optoelectronic applications based on SnO_2.

Experimental Procedure

The starting solutions were prepared from tin II chloride dihydrate (purchased from Sigma Aldrich), ethanol, methanol and distilled water. The salt was of analytical grade and was used as purchased without any further purification. All the solutions were 0.1 M in concentration. Soda lime glass substrates were cleaned in dilute hydrochloric acid, alcohol and distilled water and dried in an oven before deposition at a substrate temperature of $320 \pm 5\ ^0C$ and nozzle – to – substrate distance of 23 cm. Suction-based airbrush and air blast atomization were employed for the deposition. After the deposition, the samples were annealed in a tubular furnace at temperatures ranging from of 500 ^oC.

The RBS experiment was performed using the 1.7 MeV Pelletron Tandem Accelerator at the Centre for Energy Research & Development, Obafemi Awolowo University, Ile-Ife, Nigeria. The resulting spectra was fitted using Windows SIMNRA software for the estimation of composition and thickness of the films. Crystal structures of the film was determined through X-ray diffraction studies carried out with an X-ray Diffractometer model Bruker AXS D8 Advance. The optical properties were studied using UV–Visible – NIR Spectranet Ultraviolet spectrometer model EP2000.

Composition and Thickness Determination by RBS

The RBS spectra of both th as-deposited and annealed samples are shown in Figure 1.The results of the analysis are presented in Table 1. From the analysis, it can be inferred that the annealed sets of samples of the same composition increased in

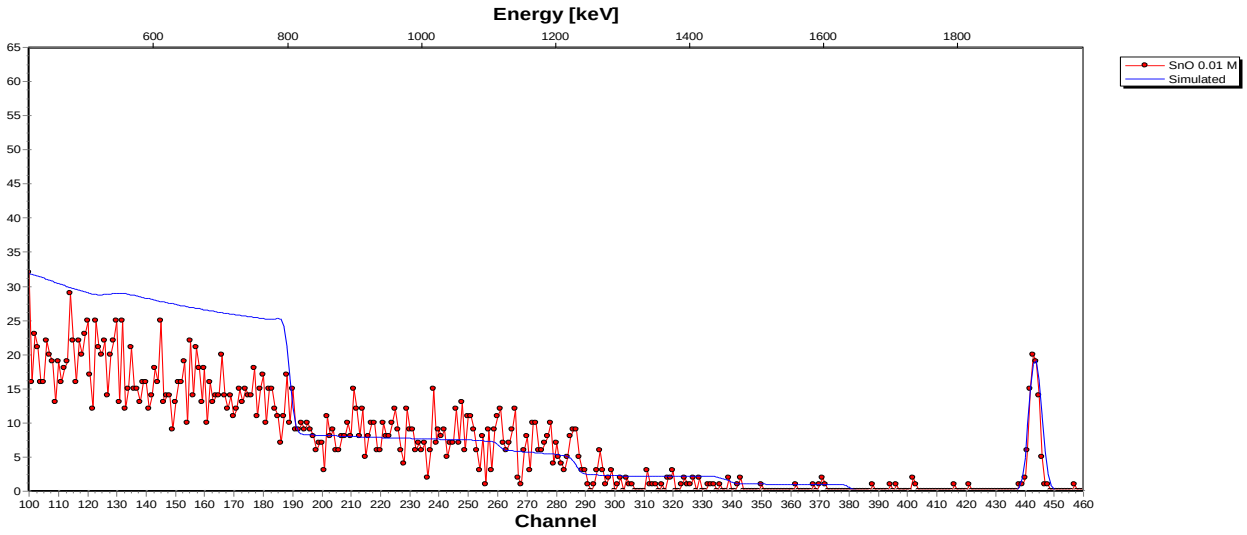

(a)

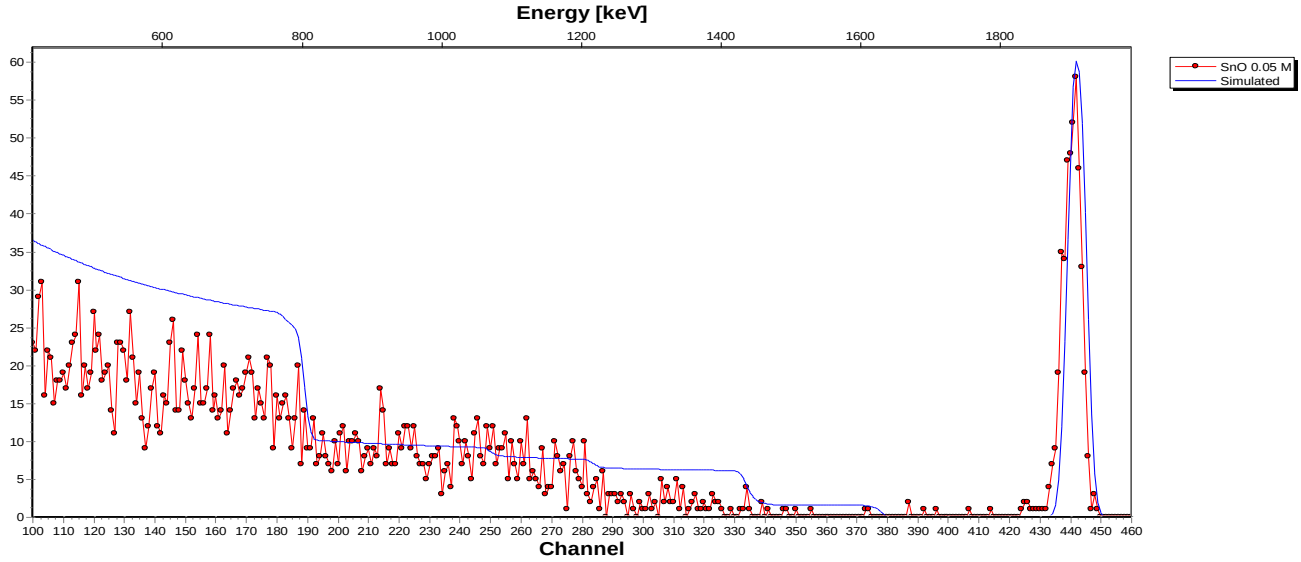

(b)

Figure 1: RBS spectrum of (a) as-deposited and (b) annealed SnO_2

Table 1: Composition and thickness of films determined from RBS analysis.

Films Compositions	Composition	Thickness (nm)
SnO_2 (as-deposited)	$Sn_{0.16}0_{0.84}$	235.35
SnO_2 (annealed)	$Sn_{0.16}0_{0.84}$	250.00

thickness compared with the as-deposited samples. This corroborated the fact that SnO_2 grains grow in size as a result of annealing (Chani *et al*., 2015).

Morphological Observation

The SEM micrographs of the films are shown in Figures 2. The particle structure is spherical in nature for both the annealed and as-deposited samples. It is also obvious that the surface of annealed films showed increased densification after annealing. Of particular importance to device applications is the porosity and the densification of the surfaces of the films. For instance the pressure – resistance relationship of a pressure transducer

could be attributed to decrease in thickness and accordingly the porosity of the sensing materials when pressure is applied. (Shen *et al*., 2018). In addition, the conductivity in metal oxides is considered to be through thermally assisted hopping transitions between spatially separated sites/particles. Hence according to Percolation theory, average conductivity depend on the concentration of sites/particles and the resistance of the path between sites. These two are affected by the porosity because with increase in pressure the concentration of sites increases and the resistance of the path decreases for a porous sample.

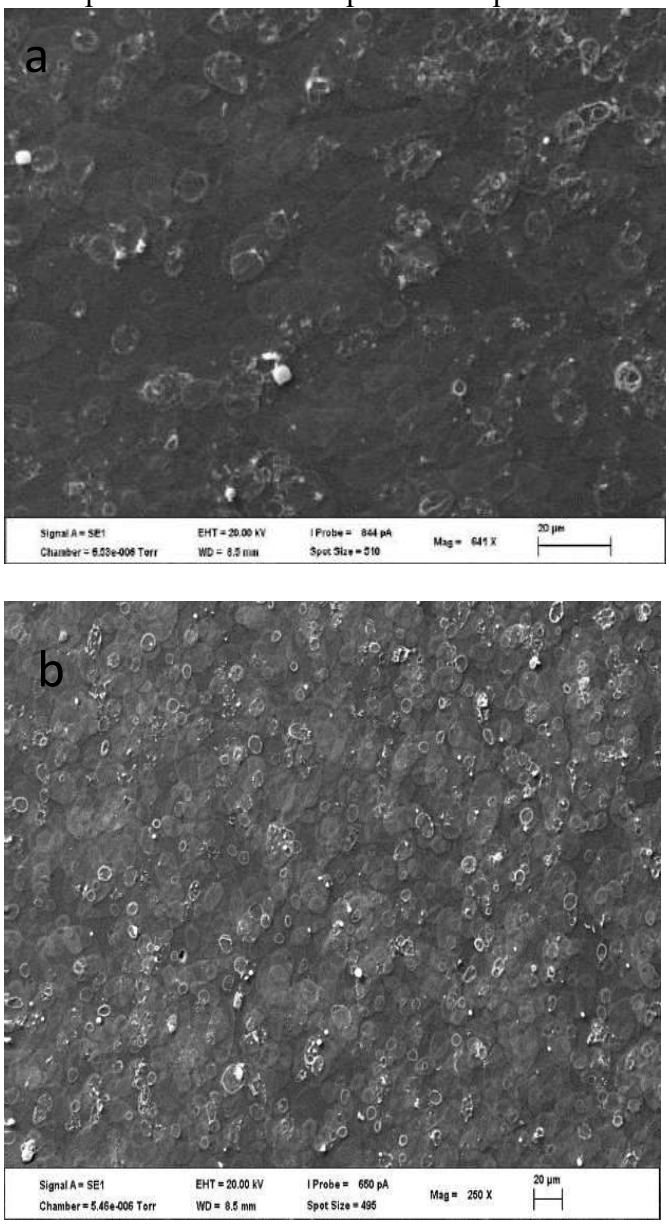

Figure 2: SEM micrograph of SnO_2 film (a) as-deposited (b) annealed

X-ray Diffraction Analysis

The X-ray diffraction patterns of the as-deposited samples were studied to confirm the crystallinity of the samples and investigate the crystal structure. The samples are crystalline in nature. The crystallite sizes were estimated using the Scherer's formula given in equation 1

$$D = {k\lambda}/{\beta cos\theta}. \qquad 1$$

Their values range from 5 to 12 nm in size. The SnO_2 is tetragonal rutile (cassiterite) in nature. The main characteristic peaks appeared at 26.7º, 38.1º and 51.8º. The indices of the peaks are (110), (200) and (211) respectively. The dominant peak is the peak at 26.6 degree, which indicates the film is textured. The results were in agreement with other studies carried out by (Summitt, 1968; Brousseau *et al*., 1997 and Sohn *et al*., 2009). The diffractograph is shown in Figure 3.

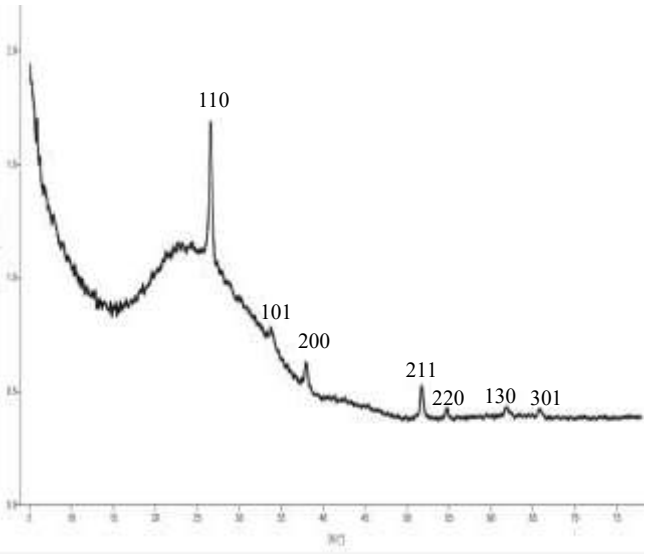

Figure 3: XRD pattern of as-deposited SnO_2

Optical analysis

The optical bandgap E_g is determined from Tauc's relation (equation 2).

$$(E) = \frac{A(h\nu - E_g)^m}{h\nu}, \qquad 2$$

where α denotes the absorption coefficient obtained by the relation given in equation 3

$$\alpha = \frac{1}{d} * (\ln\left(\frac{1}{T}\right)). \qquad 3$$

The nature of the band gaps were identified by the exponent m and an intercept of $(\alpha h\nu)^m$ plot with photon energy $h\nu$ yield the optical bandgap energy.

Figures 4 and 5 display the transmittance and the $(\alpha hv)^m$ versus hv plots, with m = 2 for direct and m = ½ for indirect bandgap transitions. The nature of the graph for SnO_2 suggests direct interband transitions with the bandgap of 3.86 eV and 3.88 eV for the as-deposited and annealed SnO_2 film respectively . The values of the calculated optical band gaps were in agreement with the range reported in the literature (3.5 – 4.0 eV), (Brousseau *et al*., 1997; Tiemann, 2007; Batal *et al.*, 2012 and Thirumala *et al*., 2014). Increase in the band gap energy is related to the improved degree of crystallization of the films with annealing (Tsay *et al*., 2015).

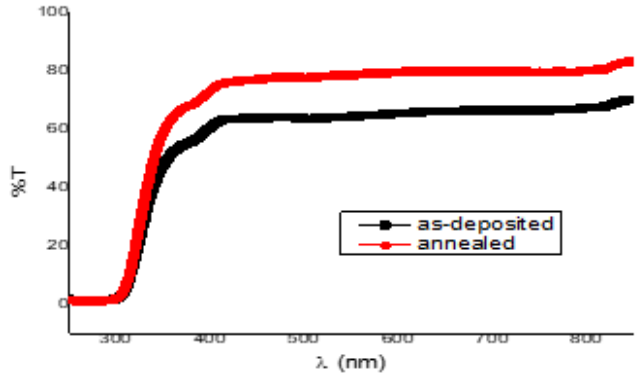

Figure 4: Transmittance of as-deposited and annealed SnO_2

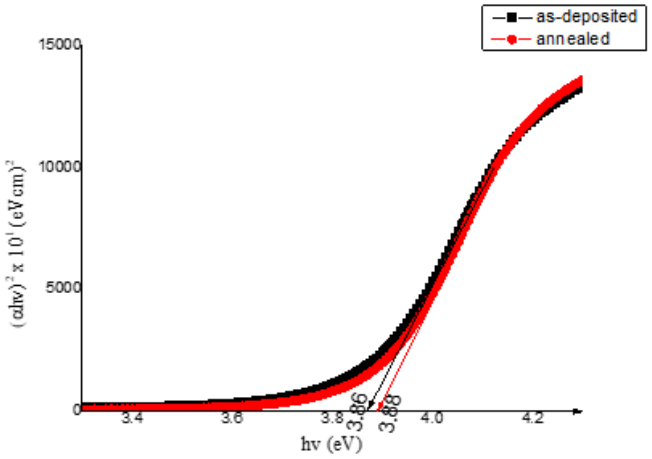

Figure 5: Optical band gap for allowed direct transition for SnO_2 (as-deposited and annealed)

Refractive Index Dispersion

Using the reflectance data derived from transmission data of both the as-deposited and annealed films and employing the relationship between reflectance and refractive index presented in equation 4 (Thirumala *et al*., 2014). The variation in the refractive index as a function of the photon wavelength was obtained. The result is presented in Figure 6 where it can be seen that annealing has led to a decrease in the refractive indices of the films. The difference between the refractive indices of the annealed and the as-deposited samples is a manifestation of the structural changes that might have occurred in the sample during the process of annealing.

$$n = \frac{1+\sqrt{R}}{1-\sqrt{R}} \qquad 4$$

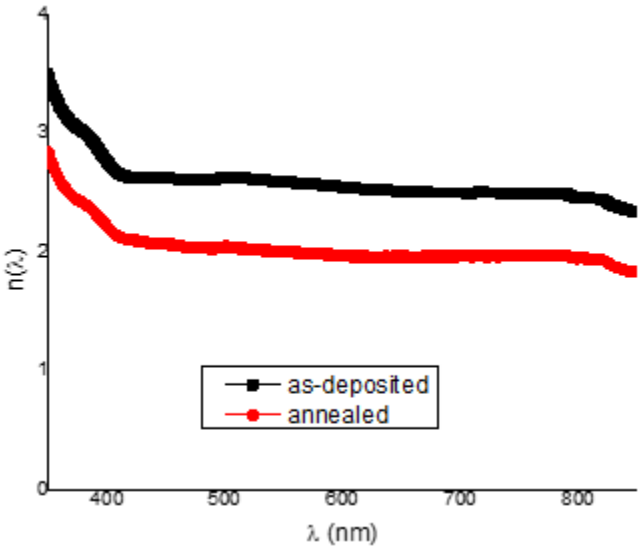

Figure 6: Refractive index versus wavelength for the as-deposited and annealed SnO_2

The transmittance data of the films were also employed to derive their complex dielectric function. The real and the imaginary parts of the dielectric function ε' and ε" are related to "n" and "k" by equation 5

$\varepsilon' = n^2 - k^2$ and $\varepsilon'' = 2nk$ 5

Moreover, if the value of n is much greater than k, then ε' is approximately equal to n^2 and the dependence of ε' on λ can be examined again using the relation in equation 6 (Wu, Li, & Sun, 2010).

$$\varepsilon' = n^2 = \varepsilon_\infty - \frac{1}{4\pi^2\varepsilon_o}\left(\frac{e^2}{c^2}\right)\left(\frac{N_c}{m^*}\right)\lambda^2 \qquad 6$$

where e is the electronic charge, c is the speed of light, N_c is the carrier density, m^* is the effective mass of the carrier and ε_∞ is the high-frequency dielectric constant. From the plot of n^2 as a function of λ^2, the intersection at $\lambda^2 = 0$ for the linear part of

the curve at higher wavelength gives the high frequency dielectric constant ε_∞ as shown in Figure 7.

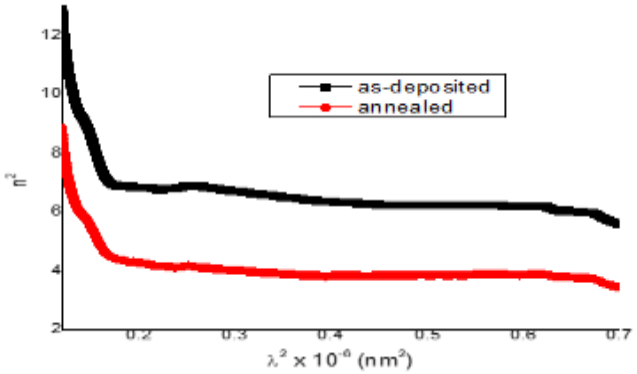

Figure 7: Plot showing the determination of the high-frequency dielectric constant (ε_α) for the as-deposited and annealed SnO_2

Oscillator strength determination

The single-term Sellmier long wavelength approximation relation given in equation 7 is used to evaluate the various oscillator parameters (Wu *et al*., 2010 and Tsay & Liang, 2015).

$$n^2(\lambda) - 1 = \frac{S_o\lambda_o^2}{\left[1-\left(\frac{\lambda_o}{\lambda}\right)^2\right]} \qquad 7$$

Where λ_o is the average oscillator parameter and So is the average oscillator strength. The plot of $(n^2(\lambda) - 1)^{-1}$ as a function of λ^{-2} given in figure 8 give a straight line where the values of $1/S_o$ and $1/S_o\lambda_o^2$ were evaluated from the slope and the intercept respectively. The dispersion parameter (E_o/S_o) for the film was also evaluated using equation 8.

$$E_o = \frac{\hbar c}{e\lambda_o} \qquad 8$$

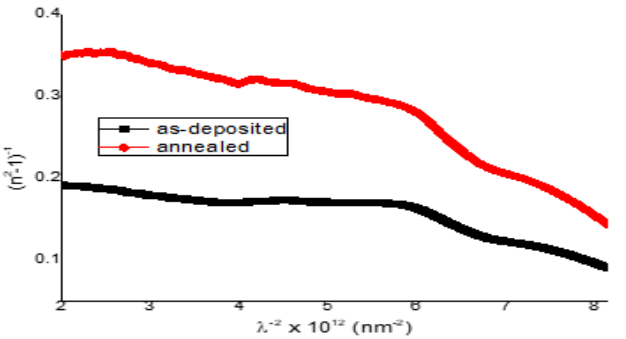

Figure 8: Plot to determine the average oscillator strength and the oscillator parameters for as-deposited and annealed SnO_2

The values obtained are listed in Table 2. The relationship between the refractive index and the photon energy is given by Wu *et al* (2010) and Tsay & Liang (2015)in equation 9.

$$n^2(h\nu) - 1 = \frac{E_{so}E_d}{E_{so}^2-(h\nu)^2} \qquad 9$$

where E_{so} is the single oscillator strength and E_d is the dissipation energy. By linearizing the expression and plotting $(n^2\text{-}1)^{-1}$ against $(h\nu)^2$ as shown in Figure 9

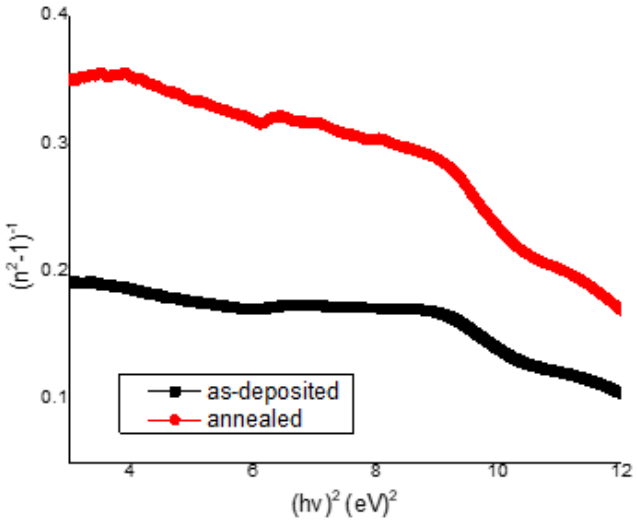

Figure 9: Plot to determine the single oscillator strength, dispersion energy, and zero frequency refractive index and the dielectric constant n_o and ε_o for as-deposited and annealed SnO_2

using the relation given in equation 10, the zero-frequency refractive index (n_o) and dielectric constant ε_o using the values of E_d and E_{so} were determined from the slope (E_{so}/E_d) and the intercept ($1/E_{so}E_d$). The results obtained from the analysis are presented in Table 2.

$$\varepsilon_o = n_o^2 = 1 + {}^{E_d}/_{E_{so}} \qquad 10$$

Tail width of localized states

The exponential tail appears because disordered and amorphous materials produced localized states extended in the bandgap. In the low photon energy, it is assumed that the spectral dependence of the absorption edge follows the empirical Urbach rule given in equation 11 (Yildirim *et al.*, 2014),

$$\propto(\nu) = \alpha_o \exp\left(\frac{h\nu}{\Delta E}\right) \qquad 11$$

Table 2: Optical constants for annealed SnO_2 films.

Optical parameters		SnO_2 (unn)	SnO_2 (ann)
Average oscillator strength	S_o	8.0x 10^{13} m^{-2}	5.0 x 10^{13} m^{-2}
Average oscillator parameter	λ_o	0.26 (μm)	0.24 (μm)
Dispersion parameter	E_o/S_o	6.25 x 10^{-14} eVm^2	1.33x 10^{-13} eVm^2
Single oscillator strength	E_{so}	5.0 eV	6.65 eV
Dispersion energy	E_d	26 eV	19 eV
High frequency dielectric constant	ε_α	6.8	4.2
Zero frequency dielectric constant	ε_o	6.13	3.78
Zero frequency refractive index	n_o	2.65	1.67

where α_o is a constant, hν is the photon energy and ΔE denotes the width of the tail of localized states in the bandgap (Urbach energy). The plot of ln (α) against the photon energy hν given in Figure 10. The linear fit was established in the linear portions of the curves. The width of the Urbach tail ΔE is the inverse of the slope of the linear fit. The results are presented in the Table 3

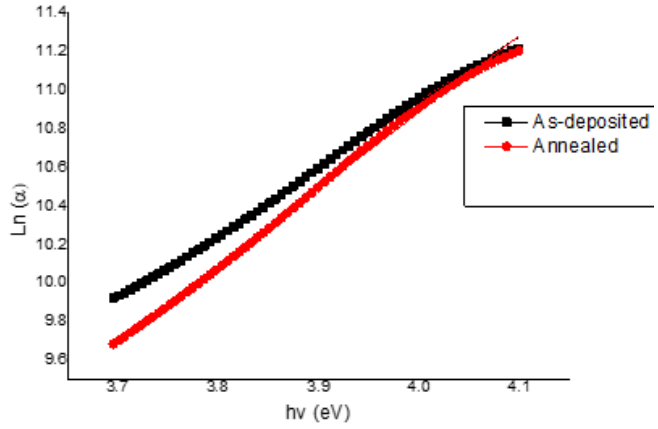

Figure 10: Ubarch tail plot for the SnO_2

Comparing these values with the values reported for SnO_2 thin films in the literature by Tiemann (2007) for spray-deposited amorphous (530 – 550 meV) and polycrystalline tin oxide (350 – 460 meV) and for vacuum-evaporated SnO_2 (483 – 646 meV) by Zeng *et al* (2010) showed that our results are a bit lower, this could be attributed to the quality of the thin films. It is also noticeable from the table that the tail width of the annealed films is lower than that of their corresponding as-deposited film. This is most probably due to the smaller density of localized states because of a decrease in disorder with annealing since crystallization becomes better with temperature. (Zhang, *et al*., 2009).

Table 3: Urbach tail energy determined for as-deposited and annealed SnO_2 films.

Films	Urbach tail width (ΔE)	Urbach tail width (ΔE)
	As-deposited	*Annealed*
SnO_2	293 meV	252meV

Conclusions

SnO_2 films were deposited on glass substrates by using facile and economical spray pyrolysis method. The properties of as-deposited and annealed films were investigated and compared. The RBS analysis showed the composition and thickness of the films. The SEM also confirmed the spherical nature of the oxide crystallites while the XRD confirmed the cassiterite and polycrystalline structure of the films. The optical band values increased with annealing from 3.86 to 3.88. We also studied the annealing effect on the tail width of the localized states in the band gap of the oxide. We observed that the Urbach tail width of the annealed films is lower than that of the as-deposited films. This is associated with a decrease in disorder as a result of annealing. We evaluated the refractive indices, zero- and high-frequency dielectric constant using the reflection data obtained from the transmission data. The high value of dielectric constant and its frequency dependence are indications of the possibility of using SnO_2 in energy storage devices and as a capacitive pressure sensing material. However, as pointed out by

Summit, (Korotcenkov, Brinzari, Schwank, DiBattista, & Vasiliev, 2001) this parameter could be well affected by structural modification. An important direction of investigation would be to study the effects of distortion of the centrosymmetric structure of this oxide on its dielectric and dispersion properties.

References

Abdullah , M., Suhail , M., & Abbas, S. (2012). Fabrication and testing of SnO2 thin films as a gas sensor. *Archives of Appllied Science Resolution, 4*(3), 1279-1288.

Bancolo, F., Santos, G., & Quiroga, R. (2012). Fabrication and Characterization of SnO2 Nanomaterial as CO2 Gas Sensor. *International Journal of Scientific and Engineering Research, 3*, 1-6.

Batal, M., Nashed, G., & Jneed, F. (2012). Electrical properties of nanostructure tin oxide thin film doped with copper prepared by sol-gel method. *Latin America Journal of Physics Education, 6*(2), 311.

Batzill , M., & Diebold, U. (2005). The Surface and Materials Science of Tin Oxide. ,. *Progress in Surface Science, 79*(2), 47-154.

Borse, R., & Garde, A. (2008). Electrical Gas Sensing properties of SnO2 Thick Film Resistors Prepared by Screen Printing Method. *Sensors & Transducers, 97*(10), 64-73.

Brousseau, J., Bourque , H., Tessier, A., & Leblanc, R. (1997). Electrical properties and topography of SnO2 thin films prepared by reactive sputtering. *Applied Surface Science*, 351-358.

Caglar, Y., Llican, S., & Caglar, M. (2007). Single-oscillator Model and Determination of Optical Constants of Spray Pyrolyzed Amorphous SnO2 Thin Films. *58*(3), 251-256.

Chani, M., Khan, S., Asiri, A., Karimov, K., Abid , M., & Bashir, M. (2015). Influence of Pressure on the Impedance of SnO2 Nanopowder. *Optoelectronic Advanced Materials Rapid Communication, 9*(1-2), 114-119.

Chani, M., Khan, S., Karimov, K., Abid, M., Asiri, A., & Akhtar, K. (2015). Synthesis of Metal Oxide Composite Nanosheets and Their Pressure Sensing properties. *Journal of Semiconductors, 36*(2), 023002.

Chen, W., Zhou, Q., Wan, F., & Gao, T. (2012). Gas Sensing Properties and Mechanism of Nano-SnO2 Based Sensor for Hydrogen and Carbon Monoxide. *Journal of Nanomaterials*.

Edukondalu, A., Shaik, K., & Gupta, A. (1992). Optical properties of amorphous Li2O-WO3-B2O3 thin films deposited by electron beam evaporation. *Phys. D, 25*, 535.

Fasasi, , A., Ngom, B., Kana-Kana, J., & Butcher, R. (2009). Synthesis and characterisation of Gd-doped BaTiO3 thin films prepared by laser ablation for optoelectronic applications. *Journal of Physics and Chemistry of Solids, 70*(10), 1322-1329.

Galatsis,, K., Cukrov, L., Wlodarski, W., McCormick, P., Kalantar-Zadeh, K., & Comini, E. (2003). 1p- and n-type Fe-doped SnO2 Gas Sensors Fabricated by the Mechanochemical Processing Technique. *Sensors and Actuators B: Chemical, 93*(1), 562-565.

Gedanken, A., Selvan, R., Perelshtein, I., & Perkas, N. (2008). Synthesis of Hexagonal-shaped SnO2 Nanocrystals and SnO2-C Nanocomposites for Electrochemical Redox Supercapacitors. *The Journal of Physical Chemistry C, 112*(6), 1825-1830.

Gordillo, G., Moreno, L., Dela Cruz, W., Teheran, Dela Cruz, W., & Teher. (1994). Preparation and Characterization of SnO2 Thin Films Deposited by Spray Pyrolysis from SnCl2 and SnCl4 Precursors. *Thin Solid Films, 252*(1), 61-66.

Guan, Y., Wang, D., Zhou, X., Sun, P., & Wang, H. (2014). Hydrothermal preparation and gas sensing properties of Zn-doped SnO2 hierarchical architectures. *Sensors and Actuators B: Chemical, 191*, 45-52.

He, C., Xiao, Y., Dong, H., Liu, Y., Zheng, M., & Xi. (2014). Mosaic-structured SnO2@C Porous Microspheres for High-performance Supercapacitor Electrode materials. *Electrochimica Acta, 142*, 157-166.

Hu, Z., Xie, Y., Wang, Y., Mo, L., Yang, Y., & Zha. (2009). Polyaniline/SnO2 nanocomposite for Supercapacitor Applications. *Materials Chemistry and Physics, 114*(2-3), 990-995.

Ikhmayies, S., & Ahmad-Bitar, R. (2013). An Investigation of the Bandgap and Urbach Tail of Vacuum-evaporated SnO2 Thin Films. *Renewable Energy, 49*, 143-146.

Jarzebski, Z., & Morton , J. (1976). Physical Properties of SnO2 Materials III. Optical Properties. *Journal of Electrochemical Society, 123*(10), 333C-346C.

Korotcenkov, G., Brinzari, V., Schwank, J., DiBattista, M., & Vasiliev, A. (2001). Peculiarities of SnO2 Thin Film Deposition by Spray Pyrolysis for Gas Sensor Application. *Sensors and Actuators B: Chemical, 77*(1-2), 244-252.

Li, F., Song, J., Yang, H., Gan, S., Zhang, Q., Ha Yang, H., & Gan, S. (2009). One-Step Synthesis of Graphene/SnO2 Nanocomposite and Its Application in Electrochemical Supercapacitors. *Nanotechnology, 20*(45), 455602.

Lim, S., Desu, S., & Rastogi, A. (2008). Chemical spray pyrolysis deposition and characterization of p-type CuCr1-xMgxO2 transparent oxide semiconductor thin films. *Journal of Physics and Chemistry of Solids, 69*(8), 2047-2056.

Liu, K., Sakurai , M., & Aono, M. (2012). Enhancing the Humidity Sensitivity of Ga2O3/SnO2 Core/Shell Microribbon by Applying Mechanical Strain and Its Application as a Flexible Strain Sensor. *Small, 8*(23), 3599-3604.

Liu, X., Cheng, S., Liu, H., Hu, S., Zhang , D., & Ning, H. (2012). A Survey on Gas Sensing Technology. *Sensors, 12*(7), 9635-9665.

Melsheimer, J., & Ziegler, D. (1985). Band Gap Energy and Urbach Tail Studies of Amorphous, Partially Crystalline and Polycrystalline Tin Oxide. *Thin Solid Films, 129*(1), 35-47.

Natsume, Y., Sakata, H, H., & Hirayama, T. (1995). Low-temperature electrical conductivity and optical absorption edge of ZnO films prepared by chemical vapour deposition. *Physica Status Solidi (a), 148*(2), 485-495.

Park, K., Choi, Y., Kang, J., Sung, Y., & Park, J. (2011). The effect of the concentration and oxidation state of Sn on the structural and electrical properties of indium tin oxide nanowires. *Nanotechnology,, 22*(28), 285712.

Perednis, D., & Gauckler, L. (2005). Thin Film Deposition Using Spray Pyrolysis. *Journal of Electroceramics, 14*(2), 103-111.

Pusawale, S., Deshmukh, P., & Lokhande, C. (2011). Chemical Synthesis of Nanocrystalline SnO2 thin Films for Supercapacitor Application. *Applied Surface Science, 257*(22), 9498-9502.

Serin, T., Serin, N., Karadeniz, S., Sari, H., Tugluoglu, N., & Pakma, O. (2006). Electrical, Structural and Optical Properties of SnO2 Thin Films Prepared by Spray Pyrolysis. *Journal of Non-Crystalline Solids, 352*(3), 209-215.

Shen, W., Ou, T., Wang, J., Qin, T., Zhang, G., & Zhang, X. (2018). Effects of High Pressure on the Electrical Resistivity and Dielectric Properties of Nanocrystalline SnO2. *Scientific Reports, 8*(1), 5086.

Shine , S., Patil, G., Kajale, D., Chavan, D., Pawar, N., & Ahire, P. (2011). Synthesis, Characterisation and Gas Sensing Performance of SnO2 Thin Films Prepared by Spray Pyrolysis. *Bulletin of Materials Science, 34*(1), 1-9.

Sohn, J., Kim, S., Kim, Z., & Yu, Y. (2009). H2S gas sensing properties of SnO2:CuO thin film sensors prepared by e-beam evaporation. *Transactions on Electrical and Electronic Materials, 10*(4), 135-139.

Summitt, R. (1968). Infrared Absorption in Single-Crystal Stannic oxide: Optical Lattice-Vibration Modes. *Journal of Applied Physics, 39*(8), 3762-3767.

Thirumala, N., Tripathy, S., Prabeena, R., & Jahnavi, V. (2014). Tin oxide thin film synthesized by sol-gel and thermal evaporation techniques for gas sensors. *Int.J.Sci.Res, 3*, 101-105.

Tiemann, M. (2007). Porous metal oxides as gas sensors. *Chemistry-A European Journal, 13*(30), 8376-8388.

Tsay, C., & Liang, S. (2015). Fabrication of p-type conductivity in SnO2 thin films through Ga doping. *Journal of Alloys and Compounds*, 644-650.

Wang, X., Ren, S., Yang, Y., Xu, M., Cai, H., & Hao, C. (2014). Hollow SnO2 Microspheres and Their Carbon-Coated Composites for

Supercapacitors. *Colloids and Surfaces A: Physicochemical and Engineering Aspect, 444*, 26-32.

Wu, Q., Li, J., & Sun, S. (2010). Nano SnO2 Gas Sensors. *Current Nanoscience, 6*(55), 525-538.

Wu, X., Liu, Y., Jiao, Y., Zhang, Z., Qu, F., & Umar, A. (2014). Hierarchical SnO2 Nanostructures made of Intermingled Ultrathin Nanosheets for Environmental Remediation, Smart Gas Sensor, Supercapacitor Applications. *ACS applied materials and interfaces, 6*(3), 2174-2184.

Yildirim, M., Yildirim, S., & Sakar, E. (2014). Synthesis, characterization and dielectric properties of SnO2 thin films. *Spectrochimica Acta Part A: Molecular and Biomolecular Spectroscopy*, 60-65.

Zeng, W., Liu, T., & Wang, Z. (2010). Sensitivity improvement of TiO2-doped SnO2 to volatile organic compounds. *Physica E: Low-dimensional Systems and Nanostructures, 43*(2), 633-638.

Zhang , S., Shen, W., Ou, T., Wang, J., Qin, T., & Zhang, G. (2018). Effects of High Pressure on the Electrical Resistivity and Dielectric Properties of Nanocrystalline SnO2. *Scientific Reports, 8*(1), 5086.

Zhang, J., Wang, S., Wang, Y., Zhu, B., Xia, H., & Wu, S. (2009). NO2 sensing performance of SnO2 hollow-sphere sensor. *Sensors and Actuators B: Chemical, 135*(2), 610-617.